Metal-tuned ligand reactivity enables CX_2 (X= O, S) homocoupling with spectator Cu centers

M. Victoria Lorenzo Ocampo and Leslie J. Murray*

Center for Catalysis, Department of Chemistry, University of Florida, Gainesville, Florida 32611-7200, United States

ABSTRACT: Ligand non-innocence is ubiquitous in catalysis, with ligands in synthetic complexes contributing as electron reservoirs or co-sites for substrate activation. The latter chemical non-innocence is manifested in H^+ storage or relay at sites beyond the metal primary coordination sphere. Reaction of a competent CO_2-to-oxalate reduction catalyst, $[K(THF)_3](Cu_3\mathbf{SL})$ where $\mathbf{L}^{3-}$ is a tris(β-diketiminate) cyclophane, with CS_2 affords tetrathiooxalate at long reaction times or at high CS_2 concentrations, where otherwise an equilibrium is established between the starting species and a complex–CS_2 adduct, in which the CS_2 is bound to C atom on the ligand backbone. X-ray diffraction analysis of this adduct reveals no apparent metal participation, suggesting an entirely ligand-based reaction controlled by the charge state of the cluster. Thermodynamic parameters for the formation of the aforementioned C_{ligand}–CS_2 bond were experimentally determined and trends with cation Lewis acidity studied, where more acidic cations shift the equilibrium towards the adduct. Relevance of such an adduct in CO_2 reduction to oxalate by this complex is supported by DFT studies, similar effect of countercation Lewis acidity on product formation, and the homocoupled heterocumulene product speciation as determined by isotopic labeling studies. Taken together, this system extends chemical non-innocence beyond H^+ to effect catalytic transformations involving C–C bond formation and represents the rarest example of metal-ligand cooperativity; that is, spectator metal ion(s) and the ligand as the reaction center.

INTRODUCTION

Ligand cooperativity is a recurrent theme in metal-catalyzed chemical transformations. This cooperative behavior can be effected through the influence of the secondary coordination sphere, covalent linkages by the supporting ligands to the substrate (or *chemical non-innocence* / *cooperativity*) or the redox participation of the ligand (or *redox non-innocence*).[1] Of the modes of cooperativity, secondary coordination sphere effects and redox non-innocence have been widely explored synthetically and have strong precedent in enzyme systems.[1–12] Classic examples of metal-ligand redox cooperativity rely on a redox active ligand serving as a reservoir of electrons with the metal center serving as the site of the bond making and breaking events.[3,4] The opposite scenario in which the ligand serves as the reaction site for bonding changes in the substrate with the metal ion(s) as the electron reservoir has precedent in catalysis only for proton reduction.[13–17] In this extreme of ligand cooperativity, the redox state of metal species can switch reactivity on or off by altering the electron density on the reactive ligand site.[13,18,19] Intermediate cases (i.e., both metal and ligand cooperate in redox and substrate activation) are well represented in the literature. For instance, seminal work by Milstein and coworkers followed by reports from de Vries, Otten and coworkers highlighted the generality of a de- and re-aromatization sequence to effect functionalization of unsaturated functional groups, and particularly nitriles, at tridentate pincer complexes (Fig. 1a-c).[20–22]

Recently, Liaw and Lu reported that CO_2 reduction to oxalate by an iron nitrosyl complex traverses a C–N bond between a ligand N atom and CO_2 (Fig. 1d).[23]

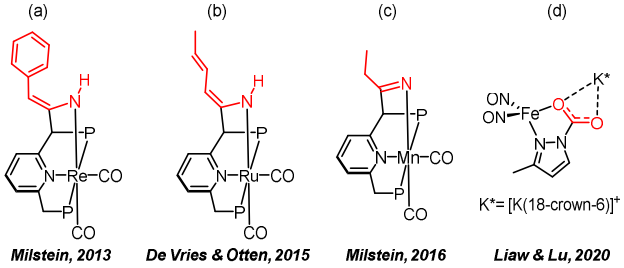

Figure 1. Intermediates involved in catalytic cycles where the ligand is covalently supporting a non-H substrate (highlighted in red).

Examples of reversible bond formation involving only ligands have been reported but not in the context of catalytic transformations. For instance, various groups have reported reversible C–C bonds between the *para*–C of aromatic ligands (*e.g.*, pyridine bound to iron(I) β-diketiminate or a perfluorophenylimidocobalt diketimide, Fig. S1).[24,25] This reaction is best described as arising from radicaloid character on the bound arene. The groups of Andersen and Chmielewski similarly reported reversible C–C bonds by a phenanthroline ytterbium complex and a pyrimidine-containing norcorrole nickel complex (Fig. S1).[26,27] Relatedly, β-diketiminates (BDIs) can also react as a nucleophile due to the contribution of the $2p_\pi$ orbital of

the γ carbon atom to the π-non-bonding HOMO (Fig. S17).[28–30] Reaction at the γ carbon typically affords addition of unsaturated substrates across the metal and ligand, analogous to the Milstein systems (Fig. S2).[31] For example, CO_2 binding to the γ-carbon of BDI complexes is reported for the main group ions Sc^{3+}, Mg^{2+} and Li^{+} (Fig. 2),[32–34] with CO_2 capture being reversible for the Sc^{3+} and Mg^{2+} compounds. Both C_γ–X bond formation and cleavage must readily occur to activate substrates and to release product in any catalytic cycle. Contrasting the tridentate meridional chelating ligands, no catalytic transformations are reported harnessing the non-innocence of BDI ligands in substrate activation.

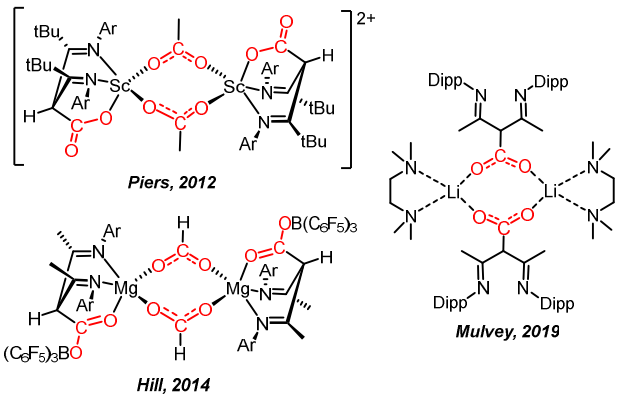

Figure 2. Structures of CO_2 adducts involving C_γ–CO_2 bond formation with BDI complexes of Sc, Mg, and Li. Fragment derived from CO_2 is depicted in red.

Among a series of reports of CO_2 reduction to oxalate, we noted that systems that achieve catalytic turnover feature coordinatively saturated metal centers (Fig. 3),[35] while coordinatively unsaturated copper centers bind to the formed oxalate and arrest after a single turnover.[36,37] In this context, our group previously reported kinetic studies of CO_2 reduction to oxalate by tricopper sulfide and selenide clusters (Cu_3SL^- and Cu_3SeL^- where L^{3-}= tris β-(diketiminate), **1**$^-$ and **2**$^-$ respectively, Fig. 3). These two catalysts display a cation and solvent dependence of the observed rate constant, wherein more Lewis acidic cations and less coordinating solvents favor the kinetics for the formation of oxalate.[38] Additionally, **2**$^-$ reacts faster than **1**$^-$, which can be explained by the stronger reducing power of the former ($E_{1/2}$ of -1.44 V and -1.58 V vs the ferrocene couple for **1** and **2**, respectively).[39,40] Herein, we report the reactivity of **1**$^-$ with the related heterocumulene, carbon disulfide, which results in a hemilabile C–C bond between substrate and ligand with no apparent interaction between the metal center and substrate. In contrast to other examples of CS_2 homocoupling to $C_2S_4^{2-}$, which are proposed to occur by a transient with CS_2 bound to the redox active metal,[41–45] we provide evidence in support of a ligand centered mechanism for the homocoupling of both CS_2 and CO_2. As a consequence, this constitutes the first report of a functional ligand with spectator redox-active metal centers, capable of catalyzing C–C coupling, a unique example of the last type of metal-ligand chemical cooperativity.

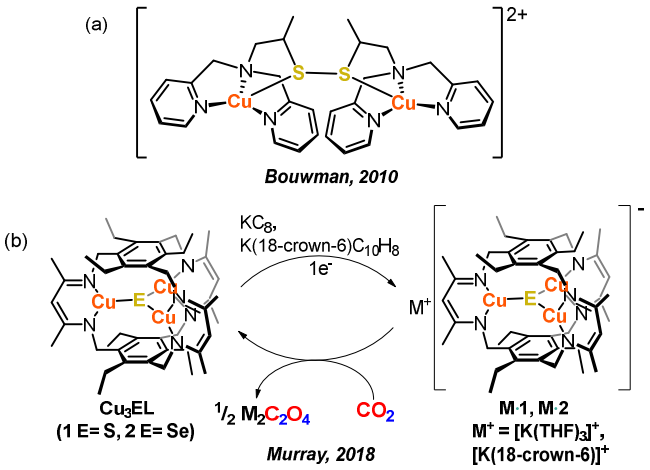

Figure 3. Cu-based molecular catalysts for reduction of CO_2 to oxalate.

RESULTS AND DISCUSSION

The addition of 22 equiv. of $^{13}CS_2$ to a 4.9 mM solution of **[K(THF)$_3$]·1** at ambient temperature in THF-d_8 afforded a green solution and a brown precipitate upon mixing. No ^{13}C labeled products were observed in the ^{13}C-NMR spectrum of the THF soluble fraction (Fig. S14). However, dissolution of the non-volatiles of this reaction in MeOH-d_4 and analysis by ^{13}C-NMR spectroscopy reveals a signal at 270.1 ppm and supports formation of tetrathiooxalate as the only ^{13}C-labeled species (Fig. S15, S16).[46] A similar ^{13}C-NMR experiment performed at –80 °C with 4.0 mM **[K(THF)$_3$]·1** and 2.3 equiv. $^{13}CS_2$ revealed a signal at 231.9 ppm, suggestive of the formation of a dithiocarboxylate (Fig. S12).[47–51]

At ambient temperature, 0.05 mM **[K(THF)$_3$]·1** and 1 equiv. of CS_2, minimal to no reaction is observed. Upon cooling to -55 °C, a turquoise to blue color change occurs. Warming this reaction mixture to ambient temperature reverses this color change (Fig. S4), suggesting that the low-temperature species is engaged in an equilibrium with **[K(THF)$_3$]·1**.

Single crystal X-ray diffraction on blue crystals of the low temperature species, **[K(THF)$_2$]·3**, were grown at -35 °C from slow diffusion of pentane into a saturated THF solution containing excess CS_2. This structure revealed a CS_2 bound to the γ-C of one BDI arm of the ligand (Fig. 4, Scheme 1). The bond lengths and angles about the γ-C bound to CS_2 and the loss of planarity of the chelate arm match prior structures in which the γ-C of BDI metal complexes acts as a nucleophile and support a neutral diimine chelate.[30] The K^+ interacts with the installed dithiocarboxylate, two THF molecules, and an η^5-BDI of a proximal complex, to give a 1D-chain structure (Fig. S3). The structure here evokes those of the main group complexes as the Cu remains bound to the two N-atom donors, contrasting the metal ion dissociation from the diimine chelate observed by Hayton and coworkers in the reaction product of a BDI nickel complex and CS_2 (Fig. S2).[52] The Cu center in the neutral diimine arm is disordered over two positions

with 46% and 54% occupancy or $Cu_{46\%}$ and $Cu_{54\%}$, respectively (Fig. 4 and S2). $Cu_{54\%}$ is displaced from the chelate plane by 0.571 Å (vs. 0.0511 Å at the unaffected arm), whereas $Cu_{46\%}$ is displaced by 0.200 Å. The Cu–SCS distance (2.698(9) Å for $Cu_{54\%}$ and 3.11(1) for $Cu_{46\%}$) is much greater than the sum of the covalent radii (*viz.* 2.37 Å),[53] suggesting a minimal Cu–SCS interaction in the solid state. The C_γ–CS_2 bond length in **[K(THF)$_2$]·3** (Table 1) is within range of reported C–C single bonds, and comparable to the Hayton's Ni complex.[52] For comparison, the average C–C bond length of the ethyl groups on the phenyl caps is 1.528(5) Å, and the labile C–C bond in Gomberg's dimer is 1.597(4) Å.[54]

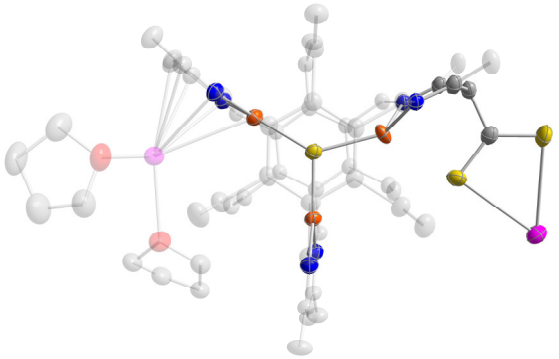

Figure 4. Single-crystal structure of **[K(THF)$_2$]·3** at 50% thermal ellipsoid depicting on only $Cu_{54\%}$. For clarity, atoms in the structure are partially transparent except for the Cu_3S cluster with the primary coordination sphere and the BDI arm bonded to CS_2. Solvent molecules of crystallization and H atoms omitted for clarity, with Cu, K, S, N and C atoms depicted as bronze, pink, yellow, blue and gray ellipsoids, respectively.

Scheme 1. Equilibrium reaction between **[K(THF)$_3$]·1** and CS_2.

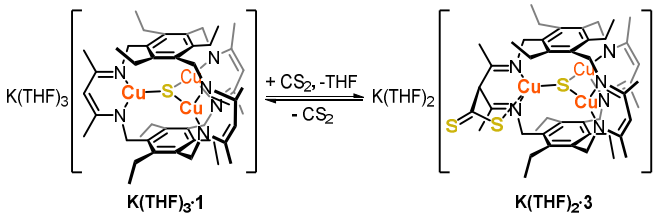

Table 1. C_{BDI}–CX_2 (X= S, O) bond lengths for **M·3** (M= $[K(THF)_2]^+$ and $[K(THF)_3]^+$), **[K(THF)$_3$]·4** and BDI-CS_2 adduct reported by Hayton and coworkers, and corresponding calculated Mayer bond orders for **[K(THF)$_3$]·3** and **[K(THF)$_3$]·4**

	d/ Å	Mayer BO
C_{BDI}–CS_2 Hayton	1.54(1)	--
C_{BDI}–CS_2 experimental	1.565(4)	--
C_{BDI}–CS_2 calculated	1.5475	0.6500
C_{BDI}–CO_2 calculated	1.6164	0.8942

Given the observed reversibility of reaction of **[K(THF)$_3$]·1** with CS_2 arising from the formation of a labile C–C bond in **[K(THF)$_2$]·3** (Scheme 1), we monitored this reaction with a large excess of CS_2 (i.e., 165 equiv.) by variable temperature UV-visible spectroscopy (VT UV-vis). At ambient temperature, new bands at 608 and 736 nm are observed together with that for the reduced complex at 695 nm. The new bands increase in intensity with concomitant decrease in that at 695 nm upon cooling to -35 °C, whereas the new bands disappear completely upon warming to 55 °C (Fig. 5 and S3). Values of K_{eq} at various temperatures were calculated by varying the equivalents of CS_2 and deconvoluting the mixture as a composite of the reduced complex and the presumed CS_2 adduct (Fig. S5, S6 and S8). Thermodynamic parameters determined from a Van't Hoff analysis are consistent with an entropically disfavored exothermic reaction (Table 2, Fig. S9). The obtained ΔH value is within the range seen for the homolytic dissociation of other labile σ C–C bonds, which span values between 26 and 84 kJ/mol, including that for Gomberg's dimer (46 kJ/mol).[26,27] Enthalpy changes are available for some of Milstein's and Fedushkin's systems,[20,22,55] but deconvoluting the contribution of metal-ligand bond is not trivial and precludes a direct comparison.

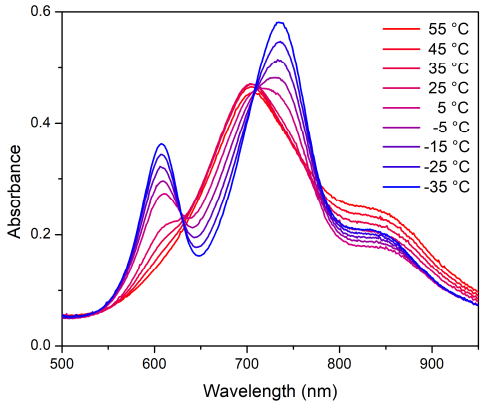

Figure 5. VT-UV-visible spectra in the range 55 to -35 °C for reaction between **[K(THF)$_3$]·1** at 0.05 mM and 165 equiv. CS_2 in THF.

Previously, our group reported that the single turnover pseudo-first order rate constants for oxalate formation from CO_2 by **1**$^-$ and **2**$^-$ increase with more Lewis acidic counterions.[38] Given that tetrathiooxalate formation observed here parallels that of CO_2 to oxalate reduction by **1**$^-$ and **2**$^-$,[38] we were curious if the equilibrium observed for CS_2 capture by **1**$^-$ was similarly sensitive to countercation identity. Therefore, we determined the equilibrium constant (K_{eq}) for formation of adduct **3**$^-$ with $[Cp^*_2Co]^+$ (Cp^*= 1,2,3,4,5-pentamethylcyclopentadienyl) as a counterion using VT UV-vis spectroscopy. Treatment of **[Cp$^*_2$Co]·1** with 40 equiv. CS_2 at ambient temperature results in no significant changes with respect to the spectrum of **1**$^-$. As for **[K(THF)$_3$]·1**, lowering the temperature results in the appearance of two new bands at 613 and 729 nm; however, these bands are only discernable at -65 °C for $[Cp^*_2Co]$·**1** and comparable conversions to those observed for **[K(THF)$_3$]·1** required substantially lower temperatures

(Fig. 6 and S7). The corresponding thermodynamic parameters highlight that the contribution of entropy dominates the effect of changing the counterion on the equilibrium constants (Table 2, Fig. S10). We hypothesize that the differences in enthalpy and entropy change for $[Cp^*_2Co]^+$ vs. K^+ as the countercation correlate with the energetic cost to reorganize the cation-complex interaction from reactant to product; that is, dissociation of K^+ from **[K(THF)$_3$]·1** in the starting material costs more vs. the less tightly-bound $[Cp^*_2Co]^+$, whereas the more localized negative charge on the dithiocarboxylate vs. **1**$^-$ afford a tighter cation-anion pair (Fig. S11).

Table 2. Thermodynamic parameters for formation of **3**$^-$ with $[K(THF)_2]^+$ and $[Cp^*_2Co]^+$ as counterions.

	$[K(THF)_2]$·3	$[Cp^*_2Co]$·3
ΔH/ kJ·mol^{-1}	-28(2)[a]	-38(1)[c]
ΔS / J·mol^{-1}·K^{-1}	-49(9)[a]	-130(5)[c]
ΔG/ kJ·mol^{-1}	-14(3)[b]	-6(2)[d]

Values determined for the temperature [a] range 248 -278 K, [b] 278 K, [c] range 178- 248 K and [d] 248 K.

Given these results with CS_2 activation and homocoupling to $C_2S_4^{2-}$, we probed whether CO_2 reduction to oxalate proceeded by a similar ligand-based pathway. Indeed, nucleophilic attack by supporting ligands was proposed in other systems as the first step towards CO_2 reduction to oxalate,[23,56] and CO_2 adducts at BDI are known (Fig. 2). However, these adducts have not exhibited further reactivity beyond reversible binding; in those cases, lack of available reducing equivalents likely precludes reductive coupling. By comparison, reversible binding to CS_2 by **1**$^-$ hints at the propensity for Cu to participate in bonding similar to *p*-block elements, supporting the covalency previously reported for the tricopper-chalcogen core,[40] and the growing evidence of Cu complexes having inverted ligand fields.[57–61] Notably, CX_2 (X= S, O) binding by **1**$^-$ can be viewed as stimuli responsive; whether the effect arises from the redox load of the complex or the change in overall charge remains to be determined.

Lack of observable intermediates and coincident pseudo-first order rate constants for formation of **1** and decay of **1**$^-$ in single turnover experiments with CO_2 have limited mechanistic studies; however, formation of tetrathiooxalate, the countercation dependence, and precedent in other BDI complexes support parallel reactivities for CS_2 and CO_2 with **1**$^-$. We reasoned then that coupling CS_2 to CO_2 could provide additional support for a common mechanism. Unfortunately, addition of CO_2 to **[K(THF)$_2$]·3** generated *in situ* with excess CS_2 affords oxalate as the only CO_2-derived product based on ^{13}C-NMR spectra (Fig. S13). The reaction rate of **[K(THF)$_3$]·1** with CO_2 and subsequent downstream steps to oxalate and **1** must be faster than reaction of **[K(THF)$_2$]·3** with CO_2 or with the analogous CO_2 adduct, **[K(THF)$_2$]·4**, which disturbs the equilibrium involving CS_2 and **[K(THF)$_3$]·1** (Scheme 1).

In addition to the possible kinetic schemes that would allow accumulation of **3**$^-$ but not the CO_2 congener, **4**$^-$, another possible reason could be a difference in equilibrium position for reaction of **[K(THF)$_3$]·1**, with CS_2 vs. CO_2; that is, in the energies of **[K(THF)$_2$]·3** and its CO_2 analog (**[K(THF)$_2$]·4**) as compared to complexes lacking the C_γ–CX_2 bond. To that end, we turned to density functional methods. Our calculations were benchmarked with our experimental results with CS_2. First, we optimized the geometry of the crystallographic coordinates of **[K(THF)$_2$]·3** in which the η^5-BDI coordination to K^+ was replaced by one or two THF molecules (abbreviated **[K(THF)$_n$]·3** and n = 3 or 4). Second, we optimized only the H-atom positions for **[K(THF)$_3$]·1** starting from the reported crystallographic coordinates. Third, we optimized a structure in which a CS_2 molecule was placed in close proximity to the K^+ ion and $[Cu_3S]^{2+}$ core in **[K(THF)$_3$]·1** (abbreviated **[K(THF)$_3$]·1+CS$_2$**). For comparison, we computed the CO_2 congeners of **[K(THF)$_n$]·3** (abbreviated **[K(THF)$_3$]·4**) and **[K(THF)$_3$]·1+CO$_2$** (Tables. S5-S10).

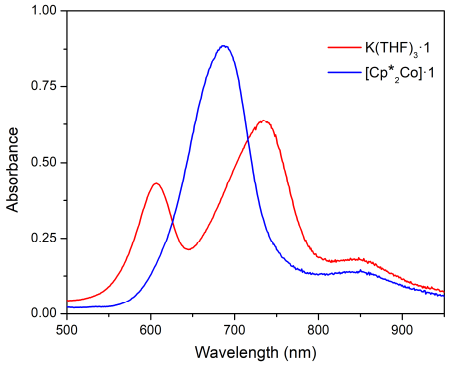

Figure 6. UV-visible spectra at -35 °C for **[K(THF)$_3$]·1** (red trace) and **[Cp$^*_2$Co]·1** (blue trace), both at 0.05 mM with 40 equiv. CS_2 in THF.

The optimized geometries for **[K(THF)$_n$]·3** with 3 or 4 THF molecules are comparable and both reproduce the main features of the crystal structure of **[K(THF)$_2$]·3**, particularly, with respect to the C_γ–CS_2 bond lengths (Table 1). One notable deviation, however, is that the computed Cu–SCS contacts are shorter than the X-ray structure (by approximately 0.5 Å) and suggestive of a coordination bond. This result is independent of the number of THF molecules bound to K^+ and the method used (*i.e.*, BP86, TPSSh, or B3LYP). Somewhat surprisingly, optimized geometries for **[K(THF)$_3$]·1+CS$_2$** afford structures in which the K^+ remains bound to one BDI arm and absence of C–C bond formation between C_γ and CS_2, with the CS_2 interacting with a Cu center and the K^+ ion. Setting all calculated species relative to **[K(THF)$_3$]·1** and free CS_2, **[K(THF)$_3$]·3** (–93.41 kJ/mol) is the lowest energy species followed by **[K(THF)$_3$]·1+CS$_2$** (–52.50 kJ/mol). Gratifyingly, these results agree with experiment as **[K(THF)$_2$]·3** is an observable intermediate upon reaction of **[K(THF)$_3$]·1** with **CS$_2$**, and with the computed and experimental C_γ–CS_2 bond energies being comparable (–40.9 kJ/mol vs. –38.1 kJ/mol). We posit that the energetic

cost to displace $[K(THF)_3]^+$ from interacting with a BDI and to interact with the dithiocarboxylate effectively makes **[K(THF)$_3$]·1+CS$_2$** a local minimum. A related question to the calculated energy differences, the calculations on **[K(THF)$_3$]·1** support that the unpaired α electron occupies an orbital of metal-BDI σ* and Cu–S π* character, consistent with prior calculations on the LUMO for neutral **1**.[39] Occupying this orbital conceivably leads to greater electron density on the BDI arms and enhanced nucleophilicity. Indeed, more negative Mulliken charges are observed on all C_γ atoms in **[K(THF)$_3$]·1** as compared to **1** (Table S3). In prior calculations on **1**, we also noted minimal mixing of the π-type non-bonding orbitals on the BDI arms with those of the cluster; for example, the three highest occupied orbitals on **1** were a pseudo *e*— and a_2— molecular orbitals almost exclusively derived from linear combinations of the BDI non-bonding π-type orbitals. By contrast, we observe substantial mixing of the cluster-based orbitals with the non-bonding π-type orbitals on the BDI arms in **[K(THF)$_3$]·1**. This greater mixing upon reduction may serve to enhance the delocalization of the electron density of the metal cluster onto C_γ of the BDI arms, thereby increasing nucleophilicity and activating the complex for reaction with CS_2 (Fig. S18).[30]

Geometry optimizations for the proposed CO_2 adduct, **[K(THF)$_3$]·4**, yields a comparable structure to the CS_2 congener except that the CO_2 carboxylate is rotated away from the copper cluster to afford Cu–O distances greater than expected for a coordination bond (Fig. 7).[62] Absence of a Cu–OCO interaction suggests that the role of the $[Cu_3S]^{2+}$ core is to tune the electronic structure of the ligand to trigger CO_2 capture by nucleophilic attack with subsequent net-homolytic C_γ–CO_2 bond cleavage to yield oxalate. Contrasting the CS_2 series, the optimized structure **[K(THF)$_3$]·1+CO$_2$** (*i.e.*, no C–C bond) is lower in energy (-41.6 kJ/mol) than **[K(THF)$_3$]·4** (–36.8 kJ/mol), referenced to the sum of the energies of **[K(THF)$_3$]·1** and CO_2. In **[K(THF)$_3$]·1+CO$_2$**, CO_2 is bound within the pocket between the K^+ and the $[Cu_3S]^{2+}$ cluster and interacts with only the K^+ center. These calculated energies agree with our inability to observe **[K(THF)$_3$]·4** in kinetic experiments (Scheme 2). Taken together with the CS_2 calculations, K^+ coordination to the CX_2 fragment in **[K(THF)$_3$]·3** and **[K(THF)$_3$]·4** are consistent with the cation and solvent dependence of the reaction rates and prior reports of CO_2 ligation to BDI complexes wherein Lewis acid coordination to the CO_2 derived carboxylate is observed.[33,38]

Forming labile C–C bonds with the ligand, which is controlled by electronic fine-tuning of the $[Cu_3S]^{2+}$ core upon reduction, evokes that reported for the release of Michael-type products from reversible coordination of nitriles to pincer ligands upon addition of Michael acceptors,[20–22] suggesting that the labile C–C bond is instrumental for productive coupling chemistry. Reaction of **1**$^-$ with heterocumulenes constitutes a rare example of functional ligand—one extreme of metal-ligand cooperativity— and in which a net one-electron reaction is initiated by a two-electron step (nucleophilic attack).[13]

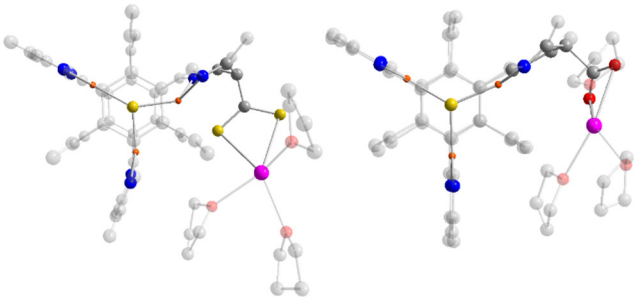

Figure 7. Geometry optimized structures for **[K(THF)$_3$]·3** (left) and **[K(THF)$_3$]·4** (right).

Scheme 2. Proposed elementary steps for reaction between **M·1** and CO_2 (M= $[K(THF)_n]^+$).

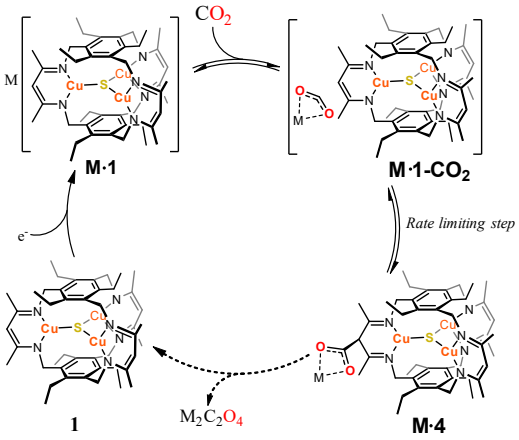

CONCLUSIONS

Reversible coordination of CS_2 to the γ-C of a BDI ligand in a $[Cu_3$-μ^3-$S]^{2+}$ cyclophanate complex, **3**$^-$, is reported. The formation of this labile C–C bond was studied by VT-UV-visible spectroscopy, and the product characterized by single crystal X-ray diffraction, and NMR methods. DFT calculations performed on the CS_2 adduct agree with experimental data, with **3**$^-$ being lower in energy than the reactants, **1**$^-$ and CS_2. Similar calculations on a CO_2 analogue of **3**$^-$ reveal that a comparable structure, **4**$^-$,is energetically accessible, albeit destabilized vs. the outer sphere CO_2 associated complex by 4.8 kJ/mol. In the CO_2 adduct **4**$^-$, the CO_2 fragment is twisted away from the copper cluster, suggesting no active involvement of the $[Cu_3S]^{2+}$ core in CO_2 trapping. In light of these results, we infer that the CO_2 adduct is an intermediate in the reduction of carbon dioxide to oxalate by **1**$^-$ and **2**$^-$. To gauge the relevance of the computationally observed CO_2 adduct, **4**$^-$, in the mechanism to form oxalate, we searched for and successfully identified tetrathiooxalate by ^{13}C-NMR in reactions with $^{13}CS_2$, further supporting analogous mechanisms in play for reduction of both heterocumulenes. These results therefore highlight the relevance of ligand cooperativity in catalysis, and in particular of the underrepresented extreme of functional ligands with spectator metals.

ASSOCIATED CONTENT

Supporting Information. Experimental details, VT UV-vis data, detailed thermodynamic calculations, ^{13}C-NMR data, Mulliken charges, calculated MO representations, crystallographic data, DFT optimized coordinates. This material is available free of charge at http://pubs.acs.org.

AUTHOR INFORMATION

Corresponding Author

* E-mail: murray@chem.ufl.edu

ORCID

Leslie J. Murray: 0000-0002-1568-958X

Author Contributions

All authors have given approval to the final version of the manuscript.

Notes

The authors declare no conflicts of interest.

ACKNOWLEDGMENT

We gratefully acknowledge the US Department of Energy (DE-SC022174) and S. N. MacMillan for the XRD data. M.V.L.O. would also like to acknowledge University of Florida, College of Liberal Arts and Sciences for a Graduate Research Fellowship, and J. F. Torres Gonzalez for helpful discussions.

REFERENCES

(1) A. Berben, L.; Bruin, B. de; F. Heyduk, A. Non-Innocent Ligands. *Chem. Commun.* **2015**, *51* (9), 1553–1554.

(2) Stripp, S. T.; Duffus, B. R.; Fourmond, V.; Léger, C.; Leimkühler, S.; Hirota, S.; Hu, Y.; Jasniewski, A.; Ogata, H.; Ribbe, M. W. Second and Outer Coordination Sphere Effects in Nitrogenase, Hydrogenase, Formate Dehydrogenase, and CO Dehydrogenase. *Chem. Rev.* **2022**, *122* (14), 11900–11973.

(3) R. Luca, O.; H. Crabtree, R. Redox-Active Ligands in Catalysis. *Chem. Soc. Rev.* **2013**, *42* (4), 1440–1459.

(4) R. Elsby, M.; Tom Baker, R. Strategies and Mechanisms of Metal–Ligand Cooperativity in First-Row Transition Metal Complex Catalysts. *Chem. Soc. Rev.* **2020**, *49* (24), 8933–8987.

(5) Shook, R. L.; Borovik, A. S. Role of the Secondary Coordination Sphere in Metal-Mediated Dioxygen Activation. *Inorg. Chem.* **2010**, *49* (8), 3646–3660.

(6) Park, Y. J.; Ziller, J. W.; Borovik, A. S. The Effects of Redox-Inactive Metal Ions on the Activation of Dioxygen: Isolation and Characterization of a Heterobimetallic Complex Containing a Mn^{III}–(μ-OH)–Ca^{II} Core. *J. Am. Chem. Soc.* **2011**, *133* (24), 9258–9261.

(7) J. Graham, D.; K. Dogutan, D.; Schwalbe, M.; G. Nocera, D. Hangman Effect on Hydrogen Peroxide Dismutation by Fe(III) Corroles. *Chem. Commun.* **2012**, *48* (35), 4175–4177.

(8) Thammavongsy, Z.; LeDoux, M. E.; Breuhaus-Alvarez, A. G.; Seda, T.; Zakharov, L. N.; Gilbertson, J. D. Pyridinediimine Iron Dicarbonyl Complexes with Pendant Lewis Bases and Lewis Acids Located in the Secondary Coordination Sphere. *Eur. J. Inorg. Chem.* **2013**, *2013* (22–23), 4008–4015.

(9) Tseng, K.-N. T.; Kampf, J. W.; Szymczak, N. K. Modular Attachment of Appended Boron Lewis Acids to a Ruthenium Pincer Catalyst: Metal–Ligand Cooperativity Enables Selective Alkyne Hydrogenation. *J. Am. Chem. Soc.* **2016**, *138* (33), 10378–10381.

(10) Delgado, M.; Ziegler, J. M.; Seda, T.; Zakharov, L. N.; Gilbertson, J. D. Pyridinediimine Iron Complexes with Pendant Redox-Inactive Metals Located in the Secondary Coordination Sphere. *Inorg. Chem.* **2016**, *55* (2), 555–557.

(11) Kita, M. R.; Miller, A. J. M. An Ion-Responsive Pincer-Crown Ether Catalyst System for Rapid and Switchable Olefin Isomerization. *Angew. Chem. Int. Ed.* **2017**, *56* (20), 5498–5502.

(12) Gordon, Z.; Drummond, M. J.; Bogart, J. A.; Schelter, E. J.; Lord, R. L.; Fout, A. R. Tuning the Fe(II/III) Redox Potential in Nonheme Fe(II)–Hydroxo Complexes through Primary and Secondary Coordination Sphere Modifications. *Inorg. Chem.* **2017**, *56* (9), 4852–4863.

(13) Bruch, Q. J.; Tanushi, A.; Müller, P.; Radosevich, A. T. Metal–Ligand Role Reversal: Hydride-Transfer Catalysis by a Functional Phosphorus Ligand with a Spectator Metal. *J. Am. Chem. Soc.* **2022**, *144* (47), 21443–21447.

(14) Wodrich, M. D.; Hu, X. Natural Inspirations for Metal–Ligand Cooperative Catalysis. *Nat. Rev. Chem.* **2017**, *2* (1), 1–7.

(15) van der Vlugt, J. I. Cooperative Catalysis with First-Row Late Transition Metals. *Eur. J. Inorg. Chem.* **2012**, *2012* (3), 363–375.

(16) Li, H.; Hall, M. B. Role of the Chemically Non-Innocent Ligand in the Catalytic Formation of Hydrogen and Carbon Dioxide from Methanol and Water with the Metal as the Spectator. *J. Am. Chem. Soc.* **2015**, *137* (38), 12330–12342.

(17) Luo, G.-G.; Zhang, H.-L.; Tao, Y.-W.; Wu, Q.-Y.; Tian, D.; Zhang, Q. Recent Progress in Ligand-Centered Homogeneous Electrocatalysts for Hydrogen Evolution Reaction. *Inorg. Chem. Front.* **2019**, *6* (2), 343–354.

(18) Annibale, V. T.; Dalessandro, D. A.; Song, D. Tuning the Reactivity of an Actor Ligand for Tandem CO_2 and C–H Activations: From Spectator Metals to Metal-Free. *J. Am. Chem. Soc.* **2013**, *135* (43), 16175–16183.

(19) Hojilla Atienza, C. C.; Milsmann, C.; Semproni, S. P.; Turner, Z. R.; Chirik, P. J. Reversible Carbon–Carbon Bond Formation Induced by Oxidation and Reduction at a Redox-Active Cobalt Complex. *Inorg. Chem.* **2013**, *52* (9), 5403–5417.

(20) Vogt, M.; Nerush, A.; Iron, M. A.; Leitus, G.; Diskin-Posner, Y.; Shimon, L. J. W.; Ben-David, Y.; Milstein, D. Activation of Nitriles by Metal Ligand Cooperation. Reversible Formation of Ketimido- and Enamido-Rhenium PNP Pincer Complexes and Relevance to Catalytic Design. *J. Am. Chem. Soc.* **2013**, *135* (45), 17004–17018.

(21) Perdriau, S.; Zijlstra, D. S.; Heeres, H. J.; de Vries, J. G.; Otten, E. A Metal–Ligand Cooperative Pathway for Intermolecular Oxa-Michael Additions to Unsaturated Nitriles. *Angew. Chem. Int. Ed.* **2015**, *54* (14), 4236–4240.

(22) Nerush, A.; Vogt, M.; Gellrich, U.; Leitus, G.; Ben-David, Y.; Milstein, D. Template Catalysis by Metal–Ligand Cooperation. C–C Bond Formation via Conjugate Addition of Non-Activated Nitriles under Mild, Base-Free Conditions Catalyzed by a Manganese Pincer Complex. *J. Am. Chem. Soc.* **2016**, *138* (22), 6985–6997.

(23) Tseng, Y.-T.; Ching, W.-M.; Liaw, W.-F.; Lu, T.-T. Dinitrosyl Iron Complex [K-18-Crown-6-Ether][$(NO)_2Fe(^{Me}PyrCO_2)$]: Intermediate for Capture and Reduction of Carbon Dioxide. *Angew. Chem.* **2020**, *132* (29), 11917–11921.

(24) Dugan, T. R.; Bill, E.; MacLeod, K. C.; Christian, G. J.; Cowley, R. E.; Brennessel, W. W.; Ye, S.; Neese, F.; Holland, P.

L. Reversible C–C Bond Formation between Redox-Active Pyridine Ligands in Iron Complexes. *J. Am. Chem. Soc.* **2012**, *134* (50), 20352–20364.

(25) Baek, Y.; Betley, T. A. Reversible C–C Bond Cleavage of a Cobalt Diketimide into an Elusive Cobalt Aryl Nitrenoid Complex. *Angew. Chem. Int. Ed.* **2022**, *61* (17), e202115437.

(26) Nocton, G.; Lukens, W. W.; Booth, C. H.; Rozenel, S. S.; Medling, S. A.; Maron, L.; Andersen, R. A. Reversible Sigma C–C Bond Formation Between Phenanthroline Ligands Activated by $(C_5Me_5)_2Yb$. *J. Am. Chem. Soc.* **2014**, *136* (24), 8626–8641.

(27) Liu, B.; Yoshida, T.; Li, X.; Stępień, M.; Shinokubo, H.; Chmielewski, P. J. Reversible Carbon–Carbon Bond Breaking and Spin Equilibria in Bis(Pyrimidinenorcorrole). *Angew. Chem. Int. Ed.* **2016**, 55 (42), 13142–13146.

(28) Webster, R. L. β-Diketiminate Complexes of the First Row Transition Metals: Applications in Catalysis. *Dalton Trans.* **2017**, *46* (14), 4483–4498.

(29) Ferreira, R. B.; Murray, L. J. Cyclophanes as Platforms for Reactive Multimetallic Complexes. *Acc. Chem. Res.* **2019**, *52* (2), 447–455.

(30) Randall, D. W.; George, S. D.; Holland, P. L.; Hedman, B.; Hodgson, K. O.; Tolman, W. B.; Solomon, E. I. Spectroscopic and Electronic Structural Studies of Blue Copper Model Complexes. 2. Comparison of Three- and Four-Coordinate Cu(II)–Thiolate Complexes and Fungal Laccase. *J. Am. Chem. Soc.* **2000**, *122* (47), 11632–11648.

(31) Camp, C.; Arnold, J. On the Non-Innocence of "Nacnacs": Ligand-Based Reactivity in β-Diketiminate Supported Coordination Compounds. *Dalton Trans.* **2016**, *45* (37), 14462–14498.

(32) LeBlanc, F. A.; Berkefeld, A.; Piers, W. E.; Parvez, M. Reactivity of Scandium β-Diketiminate Alkyl Complexes with Carbon Dioxide. *Organometallics* **2012**, *31* (3), 810–818.

(33) Anker, M. D.; Arrowsmith, M.; Bellham, P.; Hill, M. S.; Kociok-Köhn, G.; Liptrot, D. J.; Mahon, M. F.; Weetman, C. Selective Reduction of CO_2 to a Methanol Equivalent by $B(C_6F_5)_3$ -Activated Alkaline Earth Catalysis. *Chem Sci* **2014**, *5* (7), 2826–2830.

(34) Gauld, R. M.; McLellan, R.; Kennedy, A. R.; Barker, J.; Reid, J.; Mulvey, R. E. Backbone Reactivity of Lithium β-Diketiminate (NacNac) Complexes with CO_2, *t*BuNCO and *i*PrNCO. *Chem. – Eur. J.* **2019**, *25* (64), 14728–14734.

(35) Angamuthu, R.; Byers, P.; Lutz, M.; Spek, A. L.; Bouwman, E. Electrocatalytic CO_2 Conversion to Oxalate by a Copper Complex. *Science* **2010**, *327* (5963), 313–315.

(36) Farrugia, L. J.; Lopinski, S.; Lovatt, P. A.; Peacock, R. D. Fixing Carbon Dioxide with Copper:—Crystal Structure of $[LCu(\mu\text{-}C_2O_4)CuL][Ph_4B]_2$ (L = N,N',N''-Triallyl-1,4,7-Triazacyclononane). *Inorg. Chem.* **2001**, *40* (3), 558–559.

(37) Takisawa, H.; Morishima, Y.; Soma, S.; Szilagyi, R. K.; Fujisawa, K. Conversion of Carbon Dioxide to Oxalate by α-Ketocarboxylatocopper(II) Complexes. *Inorg. Chem.* **2014**, *53* (16), 8191–8193.

(38) Cook, B. J.; Di Francesco, G. N.; Abboud, K. A.; Murray, L. J. Countercations and Solvent Influence CO_2 Reduction to Oxalate by Chalcogen-Bridged Tricopper Cyclophanates. *J. Am. Chem. Soc.* **2018**, *140* (17), 5696–5700.

(39) Di Francesco, G. N.; Gaillard, A.; Ghiviriga, I.; Abboud, K. A.; Murray, L. J. Modeling Biological Copper Clusters: Synthesis of a Tricopper Complex, and Its Chloride- and Sulfide-Bridged Congeners. *Inorg. Chem.* **2014**, *53* (9), 4647–4654.

(40) Cook, B. J.; Di Francesco, G. N.; Ferreira, R. B.; Lukens, J. T.; Silberstein, K. E.; Keegan, B. C.; Catalano, V. J.; Lancaster, K. M.; Shearer, J.; Murray, L. J. Chalcogen Impact on Covalency within Molecular $[Cu_3(\mu^3\text{-}E)]^{3+}$ Clusters (E = O, S, Se): A Synthetic, Spectroscopic, and Computational Study. *Inorg. Chem.* **2018**, *57* (18), 11382–11392.

(41) Pandey, K. K. Reactivities of Carbonyl Sulfide (COS), Carbon Disulfide (CS_2) and Carbon Dioxide (CO_2) with Transition Metal Complexes. *Coord. Chem. Rev.* **1995**, *140*, 37–114.

(42) Lam, O. P.; Heinemann, F. W.; Meyer, K. C–C Bond Formation through Reductive Coupling of CS_2 to Yield Uranium Tetrathiooxalate and Ethylenetetrathiolate Complexes. *Angew. Chem. Int. Ed.* **2011**, 50 (26), 5965–5968.

(43) Lam, O. P.; Castro, L.; Kosog, B.; Heinemann, F. W.; Maron, L.; Meyer, K. Formation of a Uranium Trithiocarbonate Complex via the Nucleophilic Addition of a Sulfide-Bridged Uranium Complex to CS_2. *Inorg. Chem.* **2012**, *51* (2), 781–783.

(44) Camp, C.; Cooper, O.; Andrez, J.; Pécaut, J.; Mazzanti, M. CS_2 Activation at Uranium(III) Siloxide Ate Complexes: The Effect of a Lewis Acidic Site. *Dalton Trans.* **2015**, *44* (6), 2650–2656.

(45) Maj, J. J., Rae, A. D., Dahl, L. F. Transition Metal Promoted Carbon-Carbon Bond Formation by Reductive Dimerization of Carbon Disulfide by Reaction with the Dimeric Nickel(I) Complexes $Ni_2(\eta^5\text{-}C_5R_5)_2(\mu\text{-}CO)_2$ (R= H, Me). J. Am. Chem. Soc., **1982**, 104 (15), 4278- 4280.

(46) Tkachov, R.; Stepien, L.; Roch, A.; Komber, H.; Hennersdorf, F.; Weigand, J. J.; Bauer, I.; Kiriy, A.; Leyens, C. Facile Synthesis of Potassium Tetrathiooxalate – The "True" Monomer for the Preparation of Electron-Conductive Poly(Nickel-Ethylenetetrathiolate). *Tetrahedron* **2017**, *73* (16), 2250–2254.

(47) Rauch, M.; Parkin, G. Insertion of CS_2 into the Mg–H Bond: Synthesis and Structural Characterization of the Magnesium Dithioformate Complex, [TismPriBenz]Mg(K2-S2CH). *Dalton Trans.* **2018**, *47* (36), 12596–12605.

(48) Field, L. D.; Lawrenz, E. T.; Shaw, W. J.; Turner, P. Insertion of CO_2, CS_2, and COS into Iron(II)–Hydride Bonds. *Inorg. Chem.* **2000**, *39* (25), 5632–5638.

(49) Aust, M.; Herold, A. J.; Niederegger, L.; Schneider, C.; Mayer, D. C.; Drees, M.; Warnan, J.; Pöthig, A.; Fischer, R. A. Introducing Benzene-1,3,5-Tri(Dithiocarboxylate) as a Multidentate Linker in Coordination Chemistry. *Inorg. Chem.* **2021**, *60* (24), 19242–19252.

(50) Grote, J.; Friedrich, F.; Berthold, K.; Hericks, L.; Neumann, B.; Stammler, H.-G.; Mitzel, N. W. Dithiocarboxylic Acids: An Old Theme Revisited and Augmented by New Preparative, Spectroscopic and Structural Facts. *Chem. – Eur. J.* **2018**, *24* (11), 2626–2633.

(51) Delaude, L.; Demonceau, A.; Wouters, J. Assessing the Potential of Zwitterionic NHC·CS_2 Adducts for Probing the Stereoelectronic Parameters of N-Heterocyclic Carbenes. *Eur. J. Inorg. Chem.* **2009**, *2009* (13), 1882–1891.

(52) Hartmann, N. J.; Wu, G.; Hayton, T. W. Activation of CS_2 by a "Masked" Terminal Nickel Sulfide. *Dalton Trans.* **2016**, *45* (37), 14508–14510.

(53) Cordero, B.; Gómez, V.; Platero-Prats, A. E.; Revés, M.; Echeverría, J.; Cremades, E.; Barragán, F.; Alvarez, S. Covalent Radii Revisited. *Dalton Trans.* **2008**, No. 21, 2832–2838.

(54) Bochkarev, L. N.; Molosnova, N. E.; Zakharov, L. N.; Fukin, G. K.; Yanovsky, A. I.; Struchkov, Y. T. 1-Diphenylmethylene-4-(Triphenylmethyl)Cyclohexa-2,5-Diene Benzene Solvate. *Acta Crystallogr. C* **1995**, *51* (3), 489–491.

(55) Koptseva, T. S.; Sokolov, V. G.; Ketkov, S. Yu.; Rychagova, E. A.; Cherkasov, A. V.; Skatova, A. A.; Fedushkin, I. L. Reversible Addition of Carbon Dioxide to Main Group Metal Complexes at Temperatures about 0 °C. *Chem. – Eur. J.* **2021**, *27* (18), 5745–5753.

(56) Tanaka, K. Reduction of CO_2 Directed toward Carbon–Carbon Bond Formation. *Bull. Chem. Soc. Jpn.* **1998**, *71* (1), 17–29.

(57) Berry, J. F. Two-Center/Three-Electron Sigma Half-Bonds in Main Group and Transition Metal Chemistry. *Acc. Chem. Res.* **2016**, *49* (1), 27–34.

(58) Sarangi, R.; Yang, L.; Winikoff, S. G.; Gagliardi, L.; Cramer, C. J.; Tolman, W. B.; Solomon, E. I. X-Ray Absorption Spectroscopic and Computational Investigation of a Possible S···S Interaction in the $[Cu_3S_2]^{3+}$ Core. *J. Am. Chem. Soc.* **2011**, *133* (43), 17180–17191.

(59) Walroth, R. C.; Lukens, J. T.; MacMillan, S. N.; Finkelstein, K. D.; Lancaster, K. M. Spectroscopic Evidence for a $3d^{10}$ Ground State Electronic Configuration and Ligand Field Inversion in $[Cu(CF_3)_4]^{1-}$. *J. Am. Chem. Soc.* **2016**, *138* (6), 1922–1931.

(60) DiMucci, I. M.; Lukens, J. T.; Chatterjee, S.; Carsch, K. M.; Titus, C. J.; Lee, S. J.; Nordlund, D.; Betley, T. A.; MacMillan, S. N.; Lancaster, K. M. The Myth of d^8 Copper(III). *J. Am. Chem. Soc.* **2019**, *141* (46), 18508–18520.

(61) Hoffmann, R.; Alvarez, S.; Mealli, C.; Falceto, A.; Cahill, T. J.; Zeng, T.; Manca, G. From Widely Accepted Concepts in Coordination Chemistry to Inverted Ligand Fields. *Chem. Rev.* **2016**, *116* (14), 8173–8192.

(62) Pearson, R. G. Hard and Soft Acids and Bases. *J. Am. Chem. Soc.* **1963**, *85* (22), 3533–3539.

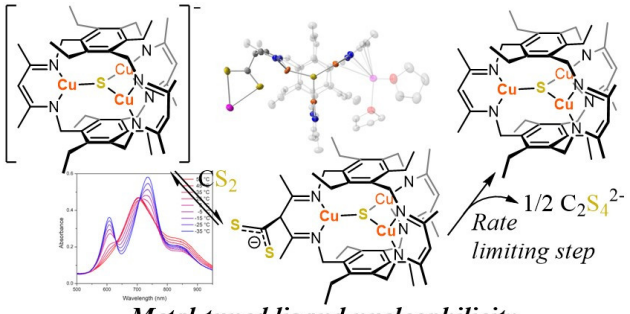

Metal-tuned ligand nucleophilicity